Synthesis and Ligand Based 3D-QSAR of 2,3-Bis-benzylidenesuccinaldehyde Derivatives as New Class Potent FPTase Inhibitor, and Prediction of Active Molecules

Min-Gyu Soung, Jong-Han Kim,[†] Byoung-Mog Kwon,[‡] and Nack-Do Sung[*]

Division of Applied Biologies and Chemistry, College of Agriculture and Life Science, Chungnam National University, Daejeon 305-764, Korea. [*]E-mail: ndsung15@hanmail.net
[†]Unigen Inc., Cheonan, Chungnam 330-863, Korea
[‡]Korea Research Institute of Bioscience and Biotechnology, Daejeon 305-600, Korea

In order to search new inhibitors against farnesyl protein transferase (FPTase), a series of 2,3-bis-benzylidenesuccinaldehyde derivatives (**1-29**) were synthesized and their inhibition activities (pI$_{50}$) against FPTase were measured. From based on the reported results that the inhibitory activities of dimers 2,3-bis-benzylidenesuccinaldehydes were higher than those of monomers cinnamaldehydes, 3D-QSARs on FPTase inhibitory activities of the dimers (**1-29**) were studied quantitatively using comparative molecular field analysis (CoMFA) and comparative molecular similarity indices analysis (CoMSIA) methods. The statistical qualities of the optimized CoMFA model II ($r^2_{cv.} = 0.693$ and $r^2_{ncv.} = 0.974$) was higher than those of the CoMSIA model II ($r^2_{cv.} = 0.484$ and $r^2_{ncv.} = 0.928$). The dependence of CoMFA models on chance correlations was evaluated with progressive scrambling analyses. And the inhibitory activity exhibited a strong correlation with steric factors of the substrate molecules. Therefore, from the results of graphical analyses on the contour maps and of predicted higher inhibitory active compounds, it is suggested that the structural distinctions and descriptors that contribute to inhibitory activities (pI$_{50}$) against FPTase will be able to applied new inhibitor design.

Key Words: 2,3-Bis-benzylidenesuccinaldehydes, 3D-QSAR, CoMFA, CoMSIA, FPTase inhibition activity

Introduction

Ras protein, which is a typical carcinogenic protein,[1] is represented as a mutational type, in 30% of human cancers.[2] Mutated forms of Ras protein are found particularly in pancreatic cancer (90%), rectal cancer (30 - 50%), and lung cancer (50%) with high frequency.[3,4] Ras protein, acts as signal messenger in cellular growth factor signal transfer process, which modulates cellular growth, proliferation and differentiation. This protein is synthesized in the cell matrix, and transformed gradually, moves into the cell membrane, at this stage, and carry out its original role.[5] Therefore in the stage of structure and activation, it is important to maintain Ras protein in the cell membrane. First stage of Ras protein transforming process is farnesylation reaction by FPTase at cystein side chain of CaaX box. Many researches about inhibitors which disturb this farnesylation reaction process are going on now.[6] Recently developed representative FPTase inhibitors are FTI276,[7] L744,382,[8] as peptidomimetics of CaaX box, clavaric acid,[9] chaetomellic acid A, B[10] which is derived from microorganism, and arteminolide[11] from plants. In addition to these, there are some other FPTase inhibitors which is under clinical experiments, such as R-115777 (IC$_{50}$ = 0.9 nM),[12] SCH-66336 (IC$_{50}$ = 2 nM)[13] and BMS-214662 (IC$_{50}$ = 0.7 nM).[14] Recently 3D-QSAR study[15] which is related to FPTase inhibition by 2-hydroxy-cinnamaldehyde derivatives being derived from cinnamon (*Cinnamomum cassia Blume*) was reported by authors. Also a new trial is attempted about the molecular docking study[16] and the regioselectivity of biogenic pathway[17] for understanding the difference of inhibi-

tion activity to FPTase protein (code name: IQBQ) between arteminolide (IC$_{50}$ = 0.36 M) and artenomaliode (IC$_{50}$ = 200 M).

According to the results[15,18] that FPTase inhibition activity of the dimer, 2,3-bis-benzylidenesuccinaldehyde is higher than that of the cinnamaldehyde monomer, we synthesized 2,3-bis-benzylidenesuccinaldehyde derivative and then the FTPase inhibition activity was measured. Also we review the structure activity relationship (SAR) with CoMFA and CoMSIA (3D-QSAR) method.[19] And we discuss about the structure characteristics which can improve the inhibition activity, and the possible high activity compounds.

Materials and Methods

Reagents and instruments. All commercial reagents and solvents were used without further purification unless otherwise specified. Solvents and reagents were purchased from Sigma-Aldrich and Fluka. Thin layer chromatography (TLC) was performed on Merck 60 F-254 silica plates and visualized by UV. Flash column chromatography was performed on silica gel (Merck, 230 - 400 mesh). Melting points were determined using Fischer-Jones melting point apparatus and are not corrected. ^{1}H-NMR spectra were measured on a Bruker AC 400 spectrometer 400 MHz or a Bruker-250 spectrometer 250 MHz in CDCl$_3$ as a solvent and TMS as an internal standard (Chemical shift in δ, ppm). Mass spectra were obtained using JMS-HX 110A/HX 100A high resolution mass spectrometer.

Synthesis of dimeric cinamaldehyde. According to author's previous report,[18] 2,3-bis-benzylidenesuccinamaldehyde

(Figure 1) derivatives (**1 - 29**) as dimeric cinnamaldehyde by reaction between 2,5-dimethoxytetrahydrofurane (2 mL, 15 mmole) and substituted (R_1, R_2 and R_3)-benzaldehyde (30 mmole) were synthesized.[20] To a solution of substituented (R_1, R_2 and R_3)-benzaldehyde (30 mmole) was added dimethoxy-tetrahydrofuran (15 mmole), potassium acetate (20 mmole), acetic acid (16 mmole) and water (2 mL). The reaction mixture was refluxed for 12 hours and cooled to room temperature. The remaining mixture was extracted with $CHCl_3$ (3 × 100 mL), washed with brine, dried over Na_2SO_4, filtered and evaporated off solvents. The residue was performed with flash chromatography on silica gel to afford pure products as a yellow oil or solid.

Here, synthetic data of compounds **1 - 20** were cited in literature[15] and the compounds **21 - 29** were synthesized in this study. Observed melting point (*Obs*. mp, °C), R_f value (TLC, *n*-hexane (*n*-Hex): ethylacetate (EtOAc)), ^{1}H-NMR spectra, yield (%) and elemental analyses are as follows.

Synthetic data of compounds (21-29).

2,3-Bis-(4-acetyloxy-3-methoxybenzylidene)succinaldehyde (21): mp 149 ~ 151 °C; R_f = 0.42 (*n*-Hex:EtOAc = 4:6); yield, 81%; ^{1}H-NMR (CDCl₃/TMS) δ 2.30 (s, 6H, O=C- C$\underline{H}_3$), 3.72 (s, 6H, -OC$\underline{H}_3$), 7.00-7.14 (m, 6H$_{arom}$), 7.68 (s, 2H, C$\underline{H}$=C-), 9.66 (s, 2H, C$\underline{H}$=O); $C_{24}H_{22}O_8$: calc.: C, 65.75, H, 5.06; found: C, 65.96, H, 4.98.

2,3-Bis-(4-valeryloxy-3-methoxybenzylidene)succinaldehyde (22): yellow oil, R_f = 0.3 (*n*-Hex:EtOAc = 4:6); yield, 70%; ^{1}H-NMR (CDCl₃/TMS) δ 0.86-1.02 (m, 6H, CH₂-C$\underline{H}_3$), 1.38-1.51 (m, 4H, C$\underline{H}_2$-CH₃), 1.64-1.78 (m, 4H, C$\underline{H}_2$-CH₂), 2.47-2.62 (m, 4H, OC$\underline{H}_2$-CH₂), 3.71 (s, 6H, -OC$\underline{H}_3$), 6.99-7.14 (m, 6H$_{arom}$), 7.27 (s, 2H, C$\underline{H}$=C-), 9.65 (s, 2H, C$\underline{H}$=O); $C_{30}H_{34}O_8$: calc.: C, 68.95, H, 6.56; found: C, 69.65, H, 6.76.

2,3-Bis-(4-benzoyloxy-3-methoxybenzylidene)succinaldehyde (23): mp 107 ~ 110 °C; R_f = 0.45 (*n*-Hex:EtOAc = 4:6); yield, 75%; ^{1}H-NMR (CDCl₃/TMS) δ 3.73 (s, 6H, -OC$\underline{H}_3$), 7.14-8.82 (m, 16H$_{aro.}$), 7.74 (s, 2H, C$\underline{H}$=C-), 9.69 (s, 2H, C$\underline{H}$=O); $C_{34}H_{26}O_8$: calc.: C, 72.59, H, 4.66; found: C, 73.12, H, 4.87.

2,3-Bis-(4-chlorobenzylidene)succinaldehyde (24): mp 172 ~ 173 °C; R_f = 0.31 (*n*-Hex: EtOAc = 6:4); yield, 15%; ^{1}H- NMR (CDCl₃/TMS) δ 7.27-7.44 (m, 8H$_{aro.}$), 7.66 (s, 2H, C$\underline{H}$=C-), 9.65 (s, 2H, C$\underline{H}$=O); $C_{18}H_{12}Cl_2O_2$: calc.: C, 65.28, H, 3.65; found: C, 65.45, H, 3.45.

2,3-Bis-(4-hydroxybenzylidene)succinaldehyde (25): mp 244 ~ 246 °C; R_f = 0.25 (*n*-Hex:EtOAc = 6:4); yield, 10%; ^{1}H-NMR (CDCl₃/TMS) δ 6.64-6.83 (m, 4H), 7.28-7.64 (m, 4H), 7.73 (s, 2H, C$\underline{H}$=C-), 9.57 (s, 2H, C$\underline{H}$=O); $C_{18}H_{14}O_4$: calc.: C, 73.46, H, 4.79; found: C, 74.16, H, 4.81.

2,3-Bis-(4-methoxybenzylidene)succinaldehyde (26): mp 204 ~ 207 °C; R_f = 0.23 (*n*-Hex:EtOAc = 6:4); yield, 15%; ^{1}H-NMR (CDCl₃/TMS) δ 3.79 (s, 6H, -OC$\underline{H}_3$), 6.70-6.93 (m, 4H), 7.39-7.61 (m, 4H), 7.64 (s, 2H, C$\underline{H}$=C-), 9.63 (s, 2H, C$\underline{H}$=O); $C_{20}H_{18}O_4$: calc.: C, 74.52, H, 5.63; found: C, 74.25, H, 5.70.

2,3-Bis-(4-propyloxybenzylidene)succinaldehyde (27): mp 152 ~ 153 °C; R_f = 0.5 (*n*-Hex: EtOAc = 6:4); yield, 75%; ^{1}H-NMR (CDCl₃/TMS) δ 0.85-1.15 (m, 6H, CH₂-C$\underline{H}_3$), 1.55-1.88 (m, 4H, C$\underline{H}_2$-CH₃), 3.80-4.04 (m, 4H, -OC$\underline{H}_2$-CH₂), 6.70-6.91 (m, 4H), 7.40-7.61 (m, 4H), 7.63 (s, 2H, C$\underline{H}$=C-), 9.62 (s, 2H, C$\underline{H}$=O); $C_{24}H_{26}O_4$: calc.: C, 76.17, H, 6.92; found: C, 75.57, H, 6.58.

2,3-Bis-(4-isopropyloxybenzylidene)succinaldehyde (28): mp 200 ~ 202 °C; R_f = 0.45 (*n*-Hex:EtOAc = 6:4); yield, 70%; ^{1}H-NMR (CDCl₃/TMS) δ 1.22-1.41 (m, 12H, C$\underline{H}_3$- CH-C$\underline{H}_3$), 4.53-4.57 (m, 2H, CH₃-C$\underline{H}$-CH₃), 6.69-6.82 (m, 4H), 7.29-7.61 (m, 4H), 7.62 (s, 2H, C$\underline{H}$=C-), 9.62 (s, 2H, C$\underline{H}$=O); $C_{24}H_{26}O_4$: calc.: C, 76.17, H, 6.92; found: C, 75.77, H, 6.82.

2,3-Bis-(4-benzoyloxybenzylidene)succinaldehyde (29): mp 207 ~ 208 °C; R_f = 0.36 (*n*-Hex: EtOAc = 6:4); yield, 65%; ^{1}H-NMR (CDCl₃/TMS) δ 7.21-8.18 (m, 18H$_{aro.}$), 7.73 (s, 2H, C$\underline{H}$=C-), 9.69 (s, 2H, C$\underline{H}$=O); $C_{32}H_{22}O_6$: calc.: C, 76.48, H, 4.41; found: C, 75.45, H, 4.27.

Biological activity measurement. FPTase inhibitory activity of 2,3-bis-benzylidene-succinamaldehyde (**1 - 29**) derivatives as substrate molecule were measured by scintillation proximity assay (SPA) method.[21] The mole concentration of 50% inhibitory activity (IC_{50}) was obtained by performing experiments at different concentrations using the method of previous report.[15] Then, the inhibition activity (pI_{50}) was counted from the inversed value of mole concentration with application of -log. The observed inhibitory activity (*Obs*.pI_{50}) of substrate molecules against FPTase was calculated from following equation (1).

$$Obs.\mathrm{p}I_{50} = -\log\left(\frac{EC_{50}\,(ppm)}{M.Wt. \times 1{,}000}\right) \tag{1}$$

Molecular modeling and prediction. 3D-QSAR analyses based on conditions and methods of previous report[15] were conducted using Sybyl software packages (Ver 8.0).[22] In order to search the most stabilized conformer of 2,3-bis-benzylidene-succinaldehyde, the energy minimization[23] were conducted by random search[24] using Tripos force field with Gästier-Hückel charge, applied X-ray data,[18] and also used to simulated annealing method.[25] Three dimensional structures of these explored substituents, which replaces the substituents (R_1 - R_3) with a H atom were set by a rigid template. And these substrate molecules were aligned on three dimensional space by the atom based fit (A) and field fit (F) alignment.[26] CoMFA and CoMSIA models from correlation analytical results between descriptors on structural characters of substrate molecules and their FPTase inhibitory activities were derived using PLS (partial least square) analysis.[27] The models for training set (n = 24) in data set compounds (n = 29) were derived and the predictabilities of each models using test set (n = 5) were discussed. The models with combination of CoMFA and CoMSIA fields per A and F alignment were derived. The best model with higher correlation ($r^2_{ncv.}$) and predictability (q^2 or $r^2_{cv.}$) among derived models was selected as an optimized model. 309 Higher active compounds were predicted in the conditions of CoMFA fields with the optimized CoMFA model II using optimizing QSAR (method: random, cycle: 1000 and best: 300) tool.[22]

Analyses of contour maps and scrambling. To analyze the visualized structural distinctions of substrate molecules, informations of the optimized CoMFA model II have expressed in three dimensional space on contour maps (steve*coeff: favor: disfavor = 80:20). And progressive scrambling was used to be validated the models, which gauges the dependence of the model on chance correlations. Optimized CoMFA models were eval-

uated with progressive scrambling analyses.[28] Thirty scrambling were carried with the conditions (maximum = 8 bins, minimum = 2 bins and critical point = 0.85). The susceptibility of the model to chance correlation can be gauged by the slope ($d_q^{2'}/dr_{yy'}^2$) of q^2 with respect to correlation of the original biological activity versus the scrambled biological activity. If a model was not dependence on chance correlation, the slope should be in the range of 0.8 - 1.2.

Results and Discussion

Biological activity. FPTase inhibition activities of the derivatives were reduced when the formyl group of 2-hydroxycinnamaldehyde[29] from cinnamon (*Cinnamomum cassia Blume*) and 2,3-bis-benzylidenesuccinaldehyde[30] was transformed into the the carboxyl or ester group. The inhibitory activities ($Obs.$ pI_{50})[18] against FPTase upon substituent changes in 2,3-bis-benzylidenesuccinaldehyde (Figure 1) derivatives (**1-29**) were determined. The predicted activity values ($Pred.pI_{50}$) by CoMFA model I and II, and the deviation ($Dev.$) between the observed and predicted values are summarized in Table 1. The compound **29** ($R_1 = R_2 =$ H, $R_3 = OCOC_6H_5$ substituent) showed the highest activity ($Obs.$ $pI_{50} = 5.62$) and the compound **12** ($R_1 = OCH_2C_6H_4$-4-NO_2, $R_2 =$ $R_3 =$ H) showed the lowest activity ($Obs.pI_{50} = 2.08$). FPTase inhibition activity value ($Obs.pI_{50}$) of the monomer cinnamal-

dehyde[15] was 2.27 ($IC_{50} = 709.70$ ppm) whereas that of the dimer 2,3-bis-benzylidenesuccinaldehyde, the compound **1**, was 3.27 ($IC_{50} = 140.86$ ppm). The inhibitory activities of dimers 2,3-bis-benzylidene-succinaldehydes were higher than monomers cinnamaldehydes.

3D-QSAR models. Table 2 illustrates the alignment conditions, as well as the statistical values of the derived models based on the combination of CoMFA and CoMSIA fields. In the case of the CoMFA model, the CoMFA model I ($r_{cv.}^2 = 0.701$ and $r_{ncv}^2 = 0.973$) under the A alignment condition was a more statistically satisfactory model than the CoMFA model II ($r_{cv.}^2 = 0.693$ and $r_{ncv.}^2 = 0.974$) under the F alignment condition. The relationships of the observed activity ($Obs.pI_{50}$) and the predicted herbicidal activity ($Pred.pI_{50}$) by the optimized CoMFA model II are shown in Figure 2. Judging from the results of the correlations (CoMFA
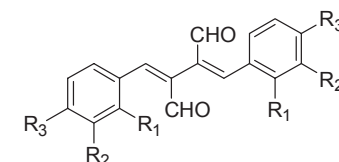

Figure 1. General structure of 2,3-bis-benzylidenesuccinaldehyde derivatives (**1−29**), dimer of cinamaldehyde as substrate molecule.

Table 1. Observed inhibitory activity ($Obs.pI_{50}$) of 2,3-Bis-benzylidenesuccinaldehydes against FTPtase and the predicted inhibitory activity ($Pred.pI_{50}$) by CoMFA models

No.	Substituents (R)			$Obs.pI_{50}$	Model I		Model II[a]	
	1 (*ortho*)	2 (*meta*)	3 (*para*)		$Pred.pI_{50}$[b]	ΔpI_{50}[c]	$Pred.pI_{50}$[b]	ΔpI_{50}[c]
1	H	H	H	3.27	3.47	−0.20	3.45	−0.18
3	Cl	H	H	4.82	4.64	0.18	4.67	0.15
4	Br	H	H	4.07	4.05	0.02	4.04	0.03
5	OCH_3	H	H	3.81	3.73	0.08	3.78	0.03
6	$OCH_2CH_2CH_3$	H	H	4.54	4.60	−0.06	4.65	−0.11
8	$OCH(CH_3)_2$	H	H	4.12	4.20	−0.08	4.30	−0.18
9	$OCH_2C_6H_5$	H	H	4.90	4.83	0.07	4.75	0.15
10	$OCH_2C_6H_4$-4-Cl	H	H	3.05	2.89	0.16	2.91	0.14
12	$OCH_2C_6H_4$-4-NO_2	H	H	2.08	2.14	−0.06	2.10	−0.02
13	H	Cl	H	4.74	4.65	0.09	4.60	0.14
14	H	$OCH_2CH_2CH_3$	H	4.91	4.94	−0.03	4.89	0.02
15	H	$OCH(CH_3)_2$	H	4.38	4.38	0.00	4.52	−0.14
16	H	$OCH_2C_6H_5$	H	5.38	5.37	0.01	5.28	0.10
17	H	OCH_3	OH	4.05	3.87	0.18	3.84	0.21
19	H	OCH_3	$OCH_2CH_2CH_3$	3.28	3.55	−0.27	3.48	−0.20
21	H	OCH_3	$OCOCH_3$	2.75	2.56	0.19	2.53	0.22
22	H	OCH_3	$OCO(CH_2)_3CH_3$	5.06	4.99	0.07	4.98	0.08
23	H	OCH_3	$OCOC_6H_5$	4.82	4.67	0.15	4.69	0.13
24	H	H	Cl	4.53	4.51	0.02	4.43	0.10
25	H	H	OH	3.54	3.76	−0.22	3.71	−0.17
26	H	H	OCH_3	3.41	3.35	0.06	3.43	−0.02
27	H	H	$OCH_2CH_2CH_3$	2.08	2.51	−0.43	2.46	−0.38
28	H	H	$OCH(CH_3)_2$	2.36	2.10	0.26	2.17	0.19
29	H	H	$OCOC_6H_5$	5.62	5.81	−0.19	5.88	−0.26

[a]Optimized CoMFA model II; [b]predicted inhibitory activity by the model; [c]different between the observed inhibitory activity and the predicted inhibitory activity.

Table 2. Summary of statistical parameters of 3D-QSAR models with two alignments

Model No.	Alignments	α^a	PLS Analyses					
			Grid (Å)	NC	$r^2_{cv.}{}^b$	$r^2_{ncv.}{}^c$	$SE_{ncv.}{}^d$	F
CoMFA I	AF	-	2.5	5	0.701	0.973	0.189	130.964
CoMFA II[e]	FF	-	2.5	5	0.693	0.974	0.187	133.599
CoMSIA I	AF	0.3	3.0	5	0.471	0.862	0.429	22.531
CoMSIA II	FF	0.6	3.0	5	0.484	0.928	0.310	46.455

Notes: AF: atom based fit; FF: field fit; NC, number of component; F, fraction of explained versus unexplained variance; [a]attenuation factor; [b]cross-validated r^2; [c]non-cross-validated r^2; [d]standard error estimate; [e]optimized model.

Table 3. Summary of relative contribution ratio (%). PRESS and Ave. of the training set and the test set with 3D-QSAR models

Model No.	Field contribution (%)			Training set		Test set	
	S	Hy	E	Hd	PRESS	Ave.	PRESS
CoMFA I	87.8	12.2	-	-	0.642	0.128	1.182
CoMFA II[a]	88.3	11.6	0.1	-	0.637	0.140	1.327
CoMSIA I	93.5	-	1.7	4.8	3.330	0.288	0.798
CoMSIA II	93.3	-	1.9	4.8	1.718	0.220	1.721

Notes: S, steric; Hy, hydrophobic; E, electrostatic; Hd, H-bond donor field; PRESS, predictive residual sum of the training set; Ave., average residual, [a]optimized model.

Table 4. Observed inhibitory activity (Obs.pI$_{50}$) of 2,3-Bis-benzylidenesuccinaldehydes against FPTase and the predicted inhibitory activity ($Pred$.pI$_{50}$) by the optimized CoMFA models for the test set compounds

No.	Substituents (R)			Obs.pI$_{50}$	CoMFA I		CoMFA II	
	1 (*ortho*)	2 (*meta*)	3 (*para*)		$Pred$.pI$_{50}{}^a$	ΔpI$_{50}{}^b$	$Pred$.pI$_{50}{}^a$	ΔpI$_{50}{}^b$
2	F	H	H	4.30	4.33	-0.03	4.35	-0.05
7	OCH$_2$CHCH$_2$	H	H	4.46	4.17	0.29	4.43	0.03
11	OCH$_2$C$_6$H$_4$-4-Br	H	H	3.58	2.75	0.83	2.81	0.77
18	H	OCH$_3$	OCH$_3$	3.17	3.39	-0.22	3.26	-0.09
20	H	OCH$_3$	OCH(CH$_3$)$_2$	3.45	2.85	0.60	2.60	0.85

[a]Predicted inhibitory activity by the models; [b]different between observed inhibitory activity and predicted inhibitory activity.
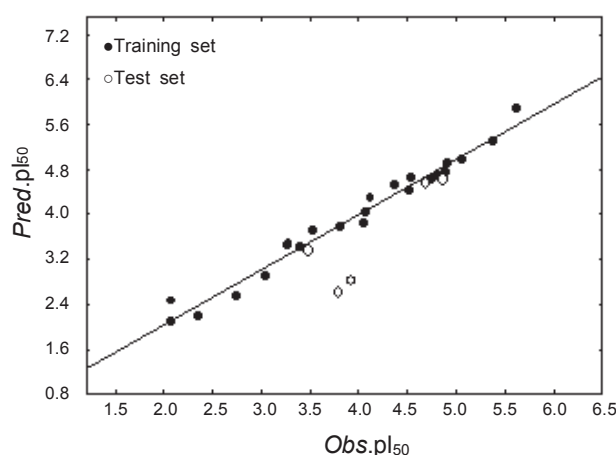

Figure 2. Relationship between the observed inhibition activity (*Obs*. pI$_{50}$) against FPTase and the predicted inhibition activity (*Pred*.pI$_{50}$) by the optimized CoMFA model II (field fit): training set: $Pred$.pI$_{50}$ = 0.974Obs.pI$_{50}$+0.103, (n = 24, s = 0.168, F = 810.644, r^2 = 0.974 & q^2 = 0.966).

model I: $Pred$.pI$_{50}$ = 0.973 Obs.pI$_{50}$+0.107, s = 0.169, F = 803.203, r^2 = 0.973, q^2 = 0.970 & CoMFA model II: $Pred$.pI$_{50}$ = 0.974Obs.pI$_{50}$+0.103, s = 0.168, F = 810.644, r^2 = 0.974 & q^2 = 0.966), the prediction and correlativity values of the CoMFA model II was more statistically satisfactory than those of the CoMFA model I. Also, the relative contribution percentages (%) of the CoMFA field were: steric field, 88.3; hydrophobic field, 11.6; electrostatic field, 0.1%. The steric field of the substrate molecule had the highest contribution values in the FPTase inhibitory activity. In the case of the CoMSIA model, the prediction and correlativity values of the CoMSIA model II ($r^2_{cv.}$ = 0.484 and $r^2_{ncv.}$ = 0.928) was more statistically satisfactory than those of the CoMSIA model I ($r^2_{cv.}$ = 0.471 and $r^2_{ncv.}$ = 0.862). The highest values of the cross-validated coefficient, $r^2_{cv.}$ (or q^2), were obtained from the CoMSIA model I with an attenuation factor (α) value of 0.3 and CoMSIA model II with an attenuation value of 0.6. The predictability ($r^2_{cv.}$ > 0.5) and correltivity ($r^2_{ncv.}$ > 0.9) value of the CoMSIA model I and II were statistically very low values.
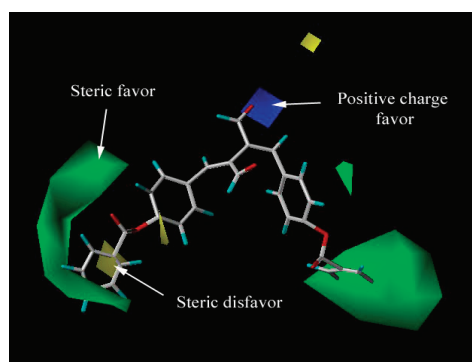
Figure 3. The contour map (steve*coeff) for the steric and electrostatic field with the optimized CoMFA model II. The most active compound (**29**) is shown in the capped sticks (favor: 80%; disfavor: 20%).
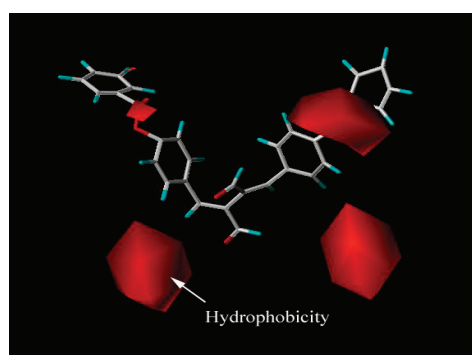

Figure 4. CoMFA-HINT contour maps (steve*coeff) for the hydrophobic field. The most active compound (**29**) is shown in the capped sticks (hydrophobic favor: 80%; hydrophilic favor: 20%).

Predictability of optimized model. The predictability and relative contribution ratio (%) of 3D-QSAR models based on two alignments were summarized in Table 3. Table 4 presents the observed values (*Obs*.pI$_{50}$) of the test set compounds, the predicted values (*Pred*.pI$_{50}$) of the 3D-QSAR analysis, and the difference values of them. To investigate the predictability of the models, the PRESS values of the training set and test set compounds and the average difference values (Ave.) of the inhibitory activity are summarized in Table 3. Statistically the best optimized model was the CoMFA model II ($r^2_{cv.}$ = 0.693, $r^2_{ncv.}$ = 0.943, PRESS = 0.637, Ave. = 0.140, and F = 133.6) in the obtained all 3D-QSAR models.

Progressive scrambling analyses. Table 5 presents three statistical values, as a valuation basis[31] on the model stability test, from the progressive scrambling analysis.[28] The progressive scrambling analysis of the CoMFA model I and II was used to calculating the prediction value (q^2) of the models, the calculated standard error of prediction (cSDEP), and the slop ($d_q^{2'}/dr^2_{yy'}$) of q^2 value. As results, the prediction values (q^2 = 0.517 & SDEP = 0.800) of the CoMFA model II was more statistically satisfactory than those of the CoMFA model I. However, the optimal value of the slop ($d_q^{2'}/dr^2_{yy'}$) of q^2 was 1.178 in the component 5 condition. This result is based on fact that the prediction value of the CoMFA model II was low, but the correlation value was more satisfactory than that of the CoMFA model I in Table 2.

CoMFA contour maps. The steric and hydrophobic field contour maps for CoMFA on the compound **29** (R_1 = H, R_2 = H, R_3 = OCOC$_6$H$_5$; *Obs*.pI$_{50}$ = 5.62), the most active inhibitor, are shown in Figure 3 and 4, respectively. According to the results of the steric field (88.3%) CoMFA contour map in Figure 3, the steric favor groups (the green polyhedra) are in the terminal area

Table 5. Model stability test for CoMFA models by progressive scrambling

Components	CoMFA I			CoMFA II ^{a}		
	$q^{2\,b}$	cSDEP^c	$d_q^{2'}/dr^2_{yy'}{}^d$	$q^{2\,b}$	cSDEP^c	$d_q^{2'}/dr^2_{yy'}{}^d$
2	0.142	0.991	0.634	0.095	1.018	0.605
3	0.492	0.779	1.740	0.448	0.811	1.682
4	0.513	0.778	1.744	0.512	0.780	1.392
5	0.571	0.761	1.857	0.517	0.800	1.178^e
6	0.563	0.776	1.895	0.530	0.808	1.444

^{a}Optimized model; $^b q^2$ = 1-(sSDEP)^2, predictability of the models; ^{c}calculated cross-validated standard error as function of correlation coefficient between the true values (y) of the dependent variables and the perturbed values (y') of the dependent variables; ^{d}slope of q^2 (cross-validated correlation coefficient from Sybyl) with respect correlation of the original dependent variables versus the perturbed dependent variables; ^{e}optimal condition.

Table 6. Predicted compounds by the optimized CoMFA Model II and their FPTase inhibitory activity

No.	Substituents (R)			*Pred*.pI$_{50}$ (IC$_{50}$)^a	ΔpI$_{50}{}^b$
	1 (*ortho*)	2 (*meta*)	3 (*para*)		
P1	Thiophene-2-yl	CH(C$_6$H$_5$)$_2$	CCH$_3$=CH$_2$	6.63 (0.20)	1.01
P2	CHBrCH$_3$	CH(C$_6$H$_5$)$_2$	CCH$_3$=CH$_2$	6.51 (0.27)	0.89
P3	OCH=CHCH$_3$	O(CH$_2$)$_8$CH$_3$	CH(CH$_3$)$_2$	6.51 (0.23)	0.89
P4	Cl	CH(CH$_3$)$_2$	C(CH$_3$)$_2$C(CH$_3$)$_3$	6.45 (0.22)	0.83
P5	CHClCH$_3$	CH(CH$_3$)$_2$	CCH$_3$=CH$_2$	6.62 (0.13)	1.00

^{a}Concentration: ppm; ^{b}difference between the observed inhibitory activity of the compound (**29**) (*Obs*.pI$_{50}$ = 5.62) and the predicted inhibitory activity (*Pred*.pI$_{50}$) by the CoMFA model II.

of the R_2 and R_3-phenyl substitutions. Thus, as the size of the R_2 and R_3-substituent rises, so does the inhibitory activity of the substituent. A positive charge favored area is represented in the blue contours in the contour map of the electrostatic field. The blue polyhedra on a formyl group indicate regions where the positive charge substituents increase the inhibitory activity. Figure 4 shows the hydrophobic field (11.6%) CoMFA contour map for the compound **29**. A hydrophobic favored area is represented in the red contours in the contour map. The red polyhedra on a R_1 and R_3-substituent of the phenyl ring indicate regions where hydrophobic substituents increase the inhibitory activity.

Prediction of active compounds. For predicting new FPTase inhibitor, we applied the CoMFA model II to the optimized QSAR tool. The prediction study was attempted according to the symmetrical arrangement of the substituent on two phenyl rings. Table 6 shows the inhibitory activities of the symmetrical substituents are higher than those of the asymmetrical analogues. The predicted inhibition activity (*Pred*.pI$_{50}$) of compounds (P1 - P5) was 6.51 - 6.63. The inhibition activity of these prediction compounds was showed higher than that of the compound **29** ($R_1 = R_2 = H$, $R_3 = OCOC_6H_5$; *Obs*.pI$_{50}$ = 5.62), the highest active compound in the training set compounds. The difference values (ΔpI$_{50}$) between the activity of the compound **29** and the prediction compounds was 0.89 - 1.01.

References

 1. Hill, B. T.; Perrin, D.; Kruczynski, A. *Crit. Rev. Oncol. Hematol.* **1997**, *33*, 7.
 2. Kelloff, G. J.; Lubet, R. A.; Fay, J. R.; Steele, V. E.; Boone, C. W.; Crowell, J. A.; Sigman, C. C. *Cancer Epidemiol., Biomarkers & Prev.* **1997**, *6*, 267.
 3. Qian, Y.; Sebti, S. M.; Hamilton, A. D. *Biopolymers* **1997**, *43*, 5.
 4. Vilella, D.; Sanchez, M.; Platas, G.; Salazar, O.; Genilloud, O.; Royo, I.; Cascales, C.; Martin, I.; Diez, T.; Silverman, K. C.; Lingham, R. B.; Singh, S. B.; Jayasuriya, H.; Pelaez, F. *J. Ind. Microbiol. Biot.* **2000**, *25*, 315.
 5. Fernandez, M.; Tundidor-Camba, A.; Caballero, J. M. *Mol. Simulat.* **2005**, *31*, 575.
 6. Gibbs, J. B.; Pompliano, D. L.; Mosser, S. D.; Rands, E.; Lingham, R. B.; Singh, S. B.; Scolnick, E. M.; Kohl, N. E.; Oliff, A. *J. Biol. Chem.* **1993**, *268*, 7617.
 7. Ohkanda, J.; Strickland, C. L.; Blaskovich, M. A.; Carrico, D.;

 8. Lockman, J. W.; Vogt, A.; Bucher, C. J.; Sun, J.; Qian, Y.; Knowles, D.; Pusateri, E. E.; Sebti, S. M.; Hamilton, A. D. *Org. Biomol. Chem.* **2006**, *4*, 482.
 8. Wesierska-Gadek, J.; Maurer, M.; Schmid, G. *J. Cellular Biochem.* **2007**, *102*, 736.
 9. Godio, R. P.; Fouces, R.; Gudina, E. J.; Martin, J. F. *Curr. Genet.* **2004**, *46*, 287.
10. Singh, S. B.; Jayasuriya, H.; Silverman, K. C.; Bonfiglio, C. A.; Williamson, J. M.; Lingham, R. B. *Bioorg. Med. Chem.* **2000**, *8*, 571.
11. Lee, S. H.; Kim, M. J.; Bok, S. H.; Lee, H. S.; Kwon, B. M.; Shin, J. H.; Seo, Y. W. *J. Org. Chem.* **1998**, *63*, 7111.
12. Martin, L. A.; Head, J. E.; Pancholi, S.; Salter, J.; Quinn, E.; Detre, S.; Kaye, S.; Howes, A.; Dowsett, M.; Johnston, S. R. *Mol. Cancer Ther.* **2007**, *6*, 2458.
13. Equbal, T.; Silakari, O.; Ravikumar, M. *Eur. J. Med. Chem.* **2008**, *43*, 204.
14. Bailey, H. H.; Alberti, D. B.; Thomas, J. P.; Mulkerin, D. L.; Binger, K. A.; Gottardis, M. M.; Martell, R. E.; Wilding, G. *Clin. Cancer Res.* **2007**, *13*, 3623.
15. Sung, N. D.; Cho, Y. K.; Kwon, B. M.; Hyun, K. H.; Kim, C. K. *Arch Pharm. Res.* **2004**, *27*, 1001.
16. Sung, N. D.; Cheun, Y. G.; Kwon, B. M.; Park, H. Y.; Kim, C. K. *Bull. Korean Chem. Soc.* **2003**, *24*, 1509.
17. Sung, N. D.; Kwon, B. M. *J. Kor. Soc. Agric. Chem. Biotechnol.* **2002**, *45*, 223.
18. Shin, D. S.; Kim, J. H.; Lee, S. K.; Han, D. C.; Son, K. H.; Kim, H. M.; Cheon, H. G.; Kim, K. R.; Sung, N. D.; Lee, S. J.; Kang, S. K.; Kwon, B. M. *Bioorg. Med. Chem.* **2006**, *14*, 2498.
19. Akamatsu, M. *Curr. Topics Med. Chem.* **2002**, *2*, 1381.
20. Ward, R. S.; Pelter, A.; Edwards, M. I.; Gilmore, J. *Tetrahedron* **1996**, *52*, 12799.
21. Reiss, Y.; Goldstein, J. L.; SEabra, M. C.; Casey, P. J.; Brown, M. S. *Cell* **1990**, *62*, 81.
22. Tripos, S. *Molecular Modeling and QSAR Software on CD-Rom* (Ver. 8.0) 2001; Tripos Associates, Inc.: 1699 S. Hanley Road, Suite 303 St. Louis, MO. 63144-2913, U.S.A.
23. Clark, M.; Van Opdenbosch, N. *J. Comput. Chem.* **1989**, *10*, 982.
24. Gilbert, K. M.; Venanzi, C. A. *J. Comput. Aided Mol. Des.* **2006**, *20*, 209.
25. Kerr, R. *Biophys. J.* **1994**, *67*, 1501.
26. Klebe, G. In *3D-QSAR Drug Design, Theory, Methods and Applications: Structural Alignment of Molecules*; Kubinyi, H., Ed.; ESCOM: Leiden, 1993; pp 173-199.
27. Cramer, R. D., III.; Bunce, J. D.; Patterson, D. E.; Frank, I. E. *Quant. Struct. Act. Relat.* **1988**, *7*, 18.
28. Clark, R. D.; Fox, P. C. *J. Comput. Aided Mol. Des.* **2004**, *18*, 563.
29. Kwon, B. M.; Cho, Y. K.; Lee, S. H.; Nam, J. Y.; Bok, S. H.; Chun, S. K.; Kim, J. A. *Planta. Med.* **1996**, *62*, 183
30. Kim, J. H. M. Sc. Thesis, Chungnam National University at Daejeon, Korea, February 2004.
31. Juan, A. A. S.; Cho, S. J. *J. Mol. Model*. **2007**, *13*, 601.